Journal of
Materials Chemistry B

PAPER

View Article Online
View Journal



Cite this: DOI: 10.1039/c8tb02917b

# Silver nanoparticles with pH induced surface charge switchable properties for antibacterial and antibiofilm applications†

Zhuangzhuang Qiao, Yan Yao, Shaomin Song, Meihui Yin and Jianbin Luo *

Received 6th November 2018,
Accepted 26th December 2018

DOI: 10.1039/c8tb02917b

rsc.li/materials-b

Silver nanoparticles (AgNPs) are widely used as antibacterial agents because of their significant antimicrobial activities and little sign of antimicrobial resistance. However, the relatively high toxicity to healthy cells and low penetration efficiency into bacterial biofilms prevent their further use in biomedical applications. In order to decrease the cytotoxicity of the AgNPs to mammalian cells while increasing their antibacterial and antibiofilm efficiency, a novel nanocomposite composed of AgNPs decorated with carboxyl betaine groups (AgNPs-LA-OB) was prepared. The zwitterion modified AgNPs showed a pH responsive transition from a negative charge to a positive charge, which enabled the AgNPs to be compatible with mammalian cells and red blood cells (RBCs) in healthy tissues (pH ~ 7.4), while strongly adhering quickly to negatively charged bacterial surfaces at infectious sites (pH ~ 5.5) based on electrostatic attraction. The AgNPs penetrated deeply into bacterial biofilms and killed the bacteria living in an acidic environment. The results indicated that the designed zwitterion NPs for antibacterial applications and eradication of bacterial biofilms, which also had particles that did not harm the healthy cells showed promise for future use in humans. The satisfactory selectivity for bacteria compared to RBCs, together with their potent eradication of bacterial biofilms make AgNPs-LA-OB a promising antibacterial nanomedicine in biomedical fields.



## 1. Introduction

With the increasing threat of microbial infections, especially in hospitals and for community acquired infections, there is a desperate need to design and develop highly effective treatment modalities to inhibit the infections.[1–4] Antibiotics have been shown to be effective in combating pathogenic microbes and have saved numerous lives in the past century.[5–7] Unfortunately, frequent and excessive use of conventional antibiotics has caused extensive multidrug resistance in bacterial infections.[8–12] Thus, it is very necessary to develop effective and safe antibacterial agents.[13–16] Silver nanoparticles (AgNPs) have been known to exhibit powerful antimicrobial activities and have been widely applied in medicine because of their high antimicrobial activity and relatively good biocompatibility.[17–23] However, the cytotoxic effects and the bactericidal activities of AgNPs remain two principal contradictions because the larger surface area and smaller size of the NPs are expected to improve the antibacterial activity; meanwhile, the mechanisms involved in the toxicity of NPs to microorganisms can also be active against mammalian cells. Generally, the relatively high toxic effects to human cells and low yield for penetration through the bacterial biofilms of AgNPs are the two main obstacles for their biomedical applications.[24]

Polymers or surfactants were coated on AgNPs to stabilize and/or to reduce its toxicity to mammalian cells. For example, AgNPs decorated on lipase-sensitive polyurethane micelles (Ag-PUM) were recently reported, which showed relatively low cytotoxicity because of the aggregation of small AgNPs into PUMs with dense poly(ethylene glycol) brushes.[25,26] The release of small AgNPs in the presence of lipase resulted in excellent antibacterial activities of AgNPs. An ultrathin layer (1–2 nm) of silver was coated onto a magnetic core with a ligand gap was prepared by Webster *et al.* to increase the penetration of AgNPs into bacterial biofilms when an external magnetic field is applied.[27] A ultrathin layer of gold was further coated onto the silver rings using another ligand gap to improve the cytotoxicity of AgNPs which also gave the NPs with a photothermal bactericidal effect.[24]

Most bacterial membranes are negatively charged whereas the mammalian cells are of negligible net charge. In addition, an acidic microenvironment is always found in bacterial infections and in bacterial biofilms.[28–30] Taking these factors into account, pH induced charge switchable AgNPs were prepared to decrease

*College of Chemistry and Environmental Protection Engineering, Southwest Minzu University, Chengdu 610041, China. E-mail: luojb1971@163.com; Tel: +86 28 85522269*

† Electronic supplementary information (ESI) available. See DOI: 10.1039/c8tb02917b

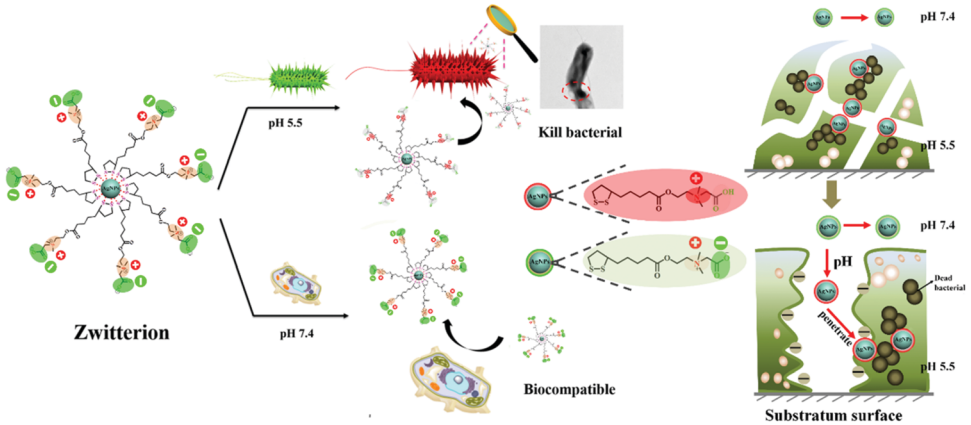


Scheme 1 Silver nanoparticles with charge switchable properties and their interaction with mammalian cells and bacteria.

their cytotoxicity towards mammalian cells in neutral solutions while increasing their toxicity to bacteria in an acidic microenvironment. To achieve this, carboxyl betaine (CB) groups were covalently bonded on the surface of AgNPs using disulfide bonds. As shown in Scheme 1, the carboxyl groups deprotonated at physiological conditions which resulted in AgNPs with zwitterions and which showed good cytocompatibilities. However, the protonation of carboxyl groups in an acidic fluid results in positively charged AgNPs, which enhance the interaction of NPs and bacteria. As far as is known, AgNPs with pH induced surface charge transform activities with an enhanced antibacterial efficiency and reduced cytotoxicity have not been reported previously.

The biofilm is a layer of bacterial cells adhered to the surface of a material or tissue with self-produced extracellular polymeric substances (EPS). The EPS serves as a protective barrier against antibiotic infiltration and cellular attack by the host's innate immune cells. It is reported that positively charged NPs show better penetration through bacterial biofilms because of the negative charge nature of EPS.[31–34] In general, the metabolic activity of bacteria is very active and diversified, and its rapid propagation is a notable feature, which causes a decrease in the local environment pH to occur at the infection site. The biofilm environment is also inconsistent, usually closer to the matrix, with a lower oxygen concentration and pH value. Surface charge adaptive gold nanoparticles or polymer micelles (capsules) have been shown to have good penetration through bacterial biofilms by taking advantage of the pH difference between the physiological environment and the bacterial biofilms.[35–37] Based on these results, it is expected that a silver-zwitterion nanocomposite will achieve better penetration through bacterial biofilms and kill the bacteria embedded in the biofilms.

# 2. Experimental

## 2.1 Materials

Silver nitrate ($AgNO_3$), *N*,*N*′-dicyclohexylcarbodiimide (DCC, 99%), 4-(dimethylamino)pyridine (4-DMAP, 99%), thioctic acid (TA, 98%) and sodium borohydride ($NaBH_4$) were obtained from Sigma-Aldrich. Dichloromethane (DCM) was dried over calcium hydride and distilled before use. *N*,*N*-Dimethylethanolamine (DMEA, Keshi, Chengdu), chloroacetic acid (J&K Scientific, Beijing), trypticase soy agar medium (TSA, AOBOX, Hengshui), trypticase soy liquid medium (TSB, AOBOX, Hengshui) were used as received. Dialysis tubing with a molecular weight cutoff of 200 and 1000 was purchased from Sinopharm Chemical Reagent (Shanghai, China).

## 2.2 Characterization

Proton nuclear magnetic resonance $^1$H-NMR spectra were obtained using a Mercury Plus 400 (Varian) NMR spectrometer at room temperature with deuterium oxide ($D_2O$) or deuterated dimethylsulfoxide (DMSO-$d_6$) as a solvent. The chemical shifts were reported in ppm relative to tetramethylsilane.

Zeta potential studies of the aqueous solution of AgNPs were carried out using a Nano-ZS 90 Nanosizer (Malvern Instruments Ltd, UK) at various pH values. No background electrolyte was added. Each measurement was repeated three times.

Ultraviolet-visible (UV-vis) studies were conducted using a UnicamUA500 UV-vis spectrophotometer (Thermo Electron Corporation) with a scan speed of 300 nm min$^{-1}$. The absorbance and transmittance spectra of the AgNPs were recorded in the range of 300–600 nm.

Inductively coupled plasma-mass spectrometry (ICP-MS) studies of the AgNPs were carried out using an Agilent 7700 ce instrument (Agilent Technologies).

Scanning electron microscope (SEM) images were taken using an Inspect F field emission scanning electron microscope (FE-SEM, FEI, USA) at 20 kV.

Transmission electron microscopy (TEM) was carried out using a Tecnai G$^2$ F20 transmission electron microscope (Royal Philips Electronics Ltd, The Netherlands) at an acceleration voltage of 200 kV.

## 2.3 The synthesis of oxibetaine (OB) and lipoic acid anhydride (LA)

In a three-necked flask, DMEA (50 mmol, 4.46 g) was dissolved in anhydrous alcohol, followed by dropwise addition of chloroacetic acid (60 mmol, 5.67 g) which was dissolved in anhydrous alcohol at

 

80 °C under vigorous stirring. The reaction was allowed to proceed under refluxing conditions for 12 h to ensure that the complete reaction had occurred. The mixture was then cooled to room temperature, followed by the addition of 500 mL of ethyl ether to start the precipitation. The crude OB was purified three times by dissolving it in anhydrous alcohol and precipitating it in ethyl ether. The residual solvent in the product was removed under vacuum for several hours to obtain pure OB.

Lipoic acid anhydride was synthesized according to a procedure reported elsewhere with slight modification.[38–41] Briefly, TA (5 mmol, 1.03 g) was dissolved in anhydrous DCM (10 mL), and DCC (3 mmol, 0.65 g) was dissolved in DCM (5 mL) at room temperature. Subsequently, the precipitate formed in the solution which was filtered to remove dicyclohexylurea. Infrared spectroscopy was used to examine the filtrate for the presence of LA (1735 and 1805 $cm^{-1}$) and the absence of the parent carboxylic acid (1701 $cm^{-1}$).

### 2.4 Synthesis of the ligand of 2-[5-(1,2-dithiolan-3-yl) pentanoyloxy]-*N*-(carboxymethyl)-*N*,*N*-dimethylethanaminium (LA-OB)

The synthesis procedure was carried out using a standard method under nitrogen protection. Briefly, an OB solution (0.028 g, 0.19 mmol) in ethyl alcohol (5.0 mL) was added to a 4-DMAP (46 mg, 0.38 mmol) solution which was dissolved in DCM (1.0 mL), and LA (0.15 g, 0.38 mmol) in DCM (1.0 mL) was then added dropwise. The mixture was stirred for 48 h at room temperature. The final product was isolated by precipitation in cold diethyl ether, washed several times with diethyl ether and then dried under a vacuum at room temperature.

### 2.5 Preparation of silver nanoparticles surface coated with carboxyl betaine (CB) groups (AgNPs-LA-OB)

Silver nanoparticles with pH induced surface charge switchable properties were synthesized using the reduction of $AgNO_3$ in the presence of LA-OB. At first, 0.05 g LA-OB was dissolved in 10 mL of water ($H_2O$) which was then mixed with 5 mL of $AgNO_3$ solution in a 20 mL sample bottle. Subsequently, $NaBH_4$ solution (2 mL) was added dropwise to the prepared solution under vigorous stirring. The specific composition of each type of AgNP is listed in Table 1. After 12 h of reduction, the solution was further purified using dialysis against $H_2O$ for 48 h. The concentration of silver in the purified solutions was determined using ICP-MS measurement.

### 2.6 Antibacterial activities against *Escherichia coli* and *Staphylococcus aureus*

Two bacterial strains, *S. aureus* (ATCC 29213) and *E. coli* (ATCC 35218), were used in this experiment. The antibacterial activities of the AgNPs-LA-OB were evaluated using minimal inhibitory concentration (MIC) and optical density (OD) readings at a wavelength of 600 nm of the microorganism solutions, which were measured every 2 h from time 0 h to 24 h using UV-vis spectrometry.[42–44] Firstly, the AgNPs-LA-OB with an initial silver concentration of 69.47 μg $mL^{-1}$ was sterilized under UV light for 2 h and diluted gradually to obtain several concentrations of AgNPs (34.74, 17.37, 8.68, 4.34, 2.17, 1.09, 0.55 μg $mL^{-1}$). Then 40 μL of bacterial solution was added and the suspensions were shaken on a shaker at 200 rpm at 37 °C. Diluted broth containing the bacterial suspension without AgNPs-LA-OB was used as the control samples.

Table 1 Feed ratios for the preparation of LA-OB coated AgNPs

| | Mass (mg) | |
|---|---|---|
| Sample | LA-OB | $AgNO_3$ |
| AgNPs–LA-OB 1 : 0.05 | 50 | 2.5 |
| AgNPs–LA-OB 1 : 0.1 | 50 | 5 |
| AgNPs–LA-OB 1 : 0.25 | 50 | 12.5 |
| AgNPs–LA-OB 1 : 0.5 | 50 | 25 |

The minimum bactericidal concentration (MBC) of an antibacterial agent were also measured and used for the evaluation of the antibacterial effects of AgNPs. Briefly, 100 μL of AgNPs-LA-OB solution was put in each zero dilution well of polystyrene 96-well plates. Adjusted bacterial suspension (50 μL) was put into each zero dilution well of a preset microplate, to achieve $5 \times 10^5$ colony forming units (CFU) $mL^{-1}$ in each well (150 μL). Bacteria were allowed to grow aerobically at 37 °C for 18 h. Subsequently, a culture suspension of 100 μL from each well was uniformly coated on plates. After overnight incubation at 37 °C, bacterial colonies became visible and the lowest concentration at which the colony formation remained absent was taken as the MBC. The experiments were repeated at least three times.

### 2.7 Biofilm culture and treatment

The biofilms of *S. aureus* were formed on Fisherbrand cover glass slides (Sanger Biotechnology Co., Ltd) according to a method published in the literature.[45,46] The *S. aureus* strains were grown aerobically in TSB broth overnight at 37 °C and the resulting bacterial suspensions were then serially diluted in TSB and adjusted to a cell density of $10^6$ CFU $mL^{-1}$. Then, 1 mL of *S. aureus* suspension was seeded into each well on which was placed a Fisher brand cover glass slide to allow the biofilm formation for seven days at 37 °C. The culture medium was refreshed every day.

Biofilm treatment was quantified in triplicate using a modified procedure that had been reported in the literature.[47–50] Briefly, the mature biofilm of *S. aureus* growing on the surface of the coverglass was gently rinsed three times with sterile phosphate buffered saline (PBS) to remove the non-adhering bacteria and then 200 μL (8.68 μg $mL^{-1}$) of AgNP–LA-OB suspension with a pH of 7.4 or 5.5 were slowly added. The control group was treated with 200 μL of 0.01 M PBS as substitute for the treatment. After incubation for 16 h contact time, the suspension was removed. A standard plate counting assay was used to assess the vitality of the residual bacteria within the biofilms. The treated biofilms were carefully rinsed three times with sterile PBS to remove the planktonic bacteria and then re-suspended in individual 10 mL polyethylene tubes containing 2 mL of physiological sterile solution were then ultrasonically mixed intermittently to detach and disaggregate the biofilm. Subsequently, the resulting suspensions were serially diluted and 100 μL diluted samples

from each tube were used to coat the plates. The plates were incubated at 37 °C for 16 h and the number of bacteria were then counted. A LIVE/DEAD BacLight Bacterial Viability kit (L-7012, Invitrogen) was used to further visually examine the anti-biofilm activities of the AgNPs-LA-OB. They were then incubated with 30 μL (3 μM) propidium iodide and SYTO-9 green fluorescent nucleic acid stain for 30 min in darkness at room temperature. Finally, the penetration of AgNPs-LA-OB, under different pH with different surface charges, into biofilms were examined using confocal laser scanning microscopy (CLSM; Olympus FV1000, Japan). Each test was carried out in triplicate.

### 2.8 SEM observation of biofilm treated with silver nanoparticles

SEM was used to visually examine the biofilm surface topography with or without the presence AgNP–LA-OB for 2 h or 16 h according to a modified protocol.[51–53] Briefly, Fisherbrand cover glass slides covered with biofilms were carefully washed three times with sterilized PBS and then 200 μL (8.68 μg $mL^{-1}$) of AgNP–LA-OB suspension in a neutral pH of 7.4 or an acidic pH of 5.5 or 4.7 environment were slowly added. The control groups were treated with 200 μL of 0.01 M PBS as substitute for the treatment. After treatment, the suspension was discarded and washed in PBS, and then fixed in 2.5% (v/v) glutaraldehyde at 4 °C for 4 h. The coverslip covered with biofilms was then dehydrated in ethanol water mixtures with increasing ethanol concentrations (50%, 70%, 85%, 90%, 95% and 100%). Finally, the biofilms were dried and examined using FE-SEM.

### 2.9 TEM study of the interaction between bacteria and AgNPs

To study of the interaction between the bacteria and the AgNPs, TEM was used to observe the morphologies of the microorganisms before and after treatment with AgNPs. The detailed procedure can be found in the literature elsewhere.[54,55] The brief methodology is: (1) the bacteria were activated by cultivating aerobically in lysogeny broth (LB) broth at 37 °C for 24 h and the activated bacteria in LB broth (5.0 mL) were centrifuged at 5000 rpm for 20 min and the supernatant was removed. (2) Then 2.0 mL of broth containing bacteria were added into the contents of the centrifuge tube again and the addition/centrifugation/removal processes were repeated. Finally, 6.0 mL of the bacterial strain was extracted. (3) Purification of bacteria. Normal saline (2.0 mL) was poured into the centrifuge tube and the residual supernatant was washed out after shaking the tube, centrifuging for 30 min and removing the supernatant. Then 2.0 mL of normal saline was added to the contents of the centrifuge tube again. After shaking well, and the bacteria were divided into two groups: experimental group (1.0 mL) and control group (1.0 mL). (4) Experimental group: the NP solution (0.5 mL; 8.68 μg $mL^{-1}$) was added to the contents of the centrifuge tube with 1.0 mL of bacteria. The mixture of bacteria and NPs was shaken well and then cultivated on a shaking bed at 37 °C for 8 h, followed by centrifugation at 5000 rpm for 30 min. The supernatant was removed and 2.0 mL of PBS was poured into the centrifuge tube. The residual supernatant was then removed after shaking the tube and centrifuging for 30 min. (5) Control group: the bacteria (1.0 mL) in another centrifuge tube without the addition of antibacterial NP solution were shaken well and then cultivated on a shaking bed at 37 °C for 8 h, followed by centrifugation at 5000 rpm for 30 min. The supernatant was removed and 2.0 mL of PBS was poured into the centrifuge tube. The tube was shaken well and centrifuged for 30 min, and then the residual supernatant was removed. (6) Immobilization of bacterial morphology. Phosphate buffer (pH 7.4; 0.5 mL) containing 2.5% glutaraldehyde was added to two centrifuge tubes of the experimental and control groups. The tubes were shaken well and then placed in the fridge overnight at 4 °C to fix the bacterial morphology. (7) TEM sample preparation. The two tubes were centrifuged for 30 min and the supernatants were removed. Then sterile water was added into both tubes. The tubes were shaken well and centrifuged for 30 min. After the removal of the super supernatant, approximately 0.5 mL of sterile water was added to both tubes. These bacterial suspensions were then shaken well and were then ready for preparation for TEM observation.

### 2.10 Hemolysis assay

All the experimental protocols used followed the guidelines of the Animal Care and Use Committee, Southwest University for Nationalities and the experiments were approved by the Committee. Healthy Kunming mice were obtained from Chengdu Dossy Experimental Animals (Chengdu, Sichuan, China). The hemolysis assays were conducted using heparin stabilized red blood cells (RBCs), which were freshly collected from the mice.[56–58] Briefly, fresh mouse whole blood was washed with PBS solution and isolated using centrifugation at 1500 rpm for 10 min. Following the last wash, the RBCs were diluted in PBS to achieve 8% blood content (by volume). The diluted RBC suspension (200 μL) was mixed with different concentrations of NP solution for a 2 h incubation period. After centrifugation to isolate the RBCs, the supernatant sample was transferred to a quartz colorimetric utensil and the spectrum was recorded using a UV-vis spectrophotometer at 570 nm. A negative control solution that contained only PBS was used as a reference for 0% hemolysis. Pure deionized water was used as positive control for hemolysis test. The percentage hemolysis of the RBCs was calculated using the following equation: percentage hemolysis = [(sample absorbance − negative control absorbance)/(positive control absorbance − negative control absorbance)] × 100. The test was repeated three times for each sample.

## 3. Results and discussion

### 3.1 Preparation and characterization of AgNP–LA-OB

In this work, a convenient, efficient strategy for the synthesis of AgNPs with pH induced surface charge transform activities (AgNP–LA-OB) was demonstrated. First the LA-OB were successfully synthesized using the three-step process illustrated in Scheme 2. After purification, the representative $^1$H-NMR spectra was obtained and the assignment of the peaks is presented in Fig. 1. The characteristic signals of OB at ~3.3 ppm, ~3.9 ppm and ~4.6 ppm whereas the signals at ~1.8 ppm and ~3.22 ppm

 

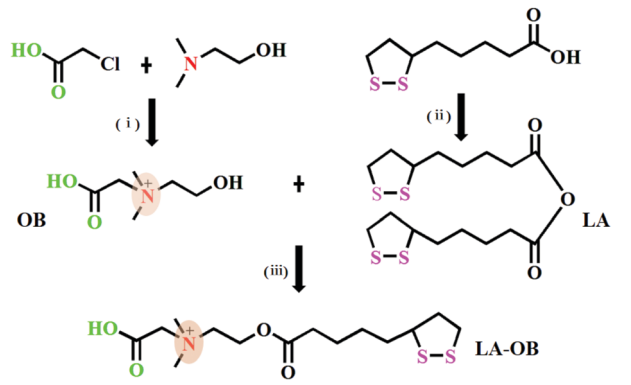


Scheme 2 Synthesis route of LA-OB.

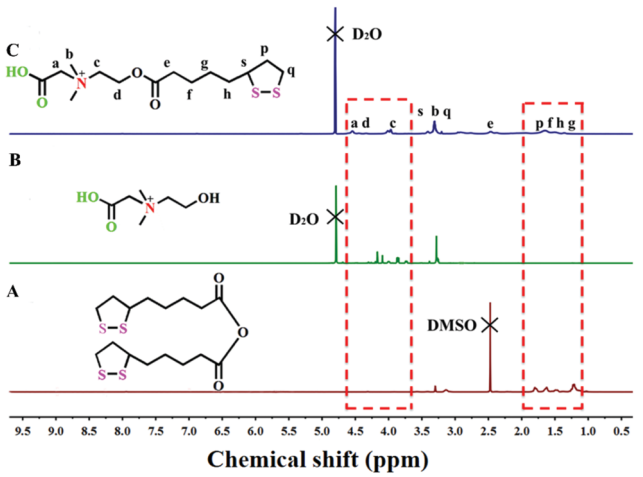


Fig. 1 $^{1}$H-NMR spectra of LA (A) in DMSO-$d_6$ and OB (B), LA-OB (C) in $D_2O$.

were assigned to the two methylene protons in the lipoic ring, which indicated the successful synthesis of surface modification agents for AgNPs (LA-OB).

Silver nanoparticles surface coated with CB groups were prepared by simply reducing the silver ions in the presence of LA-OB. The disulfide groups of LA-OB were reduced to thiol which covalently attached the CB groups onto the AgNP surface with metal–sulfur bonds. The effect of the ratio of LA–OB : silver on the size and morphology of the prepared AgNPs was studied by adding different amounts of $AgNO_3$ to the reaction mixtures. The ratio of LA–OB : silver was varied from 1 : 0.05 to 1 : 0.5 as shown in Table 1. As is known, the optical properties were closely dependent to the size and morphological features of the AgNPs. The UV-vis spectra were used to evaluate the resulting AgNPs-LA-OB prepared from different mass ratios of LA-OB and $AgNO_3$ and the results are shown in Fig. 2A and the TEM micrographs of the resulting nanocomposites are shown in Fig. 2C. It is clearly shown from the UV-vis spectra and TEM images that well distributed AgNPs with a diameter of several nanometers were obtained when the ratio of LA-OB and $AgNO_3$ was 1 : 0.1. Therefore, an AgNP–LA-OB ratio of 1 : 0.1 was used for further studies. The results of thermogravimetric analysis indicated that the amount of LA-OB grafted on AgNPs was about 38% (Fig. S1, ESI†).

The zeta potentials of the AgNP–LA-OB were determined using dynamic light scattering at 25 °C with a Nano-ZS 90 Nanosizer. As shown in Fig. 2B, at physiological conditions or above (pH > 7.4), the AgNP–LA-OB exhibited a negative surface charge because of the ionization of the carboxyl groups, suggesting that there was a long circulation time in the blood stream. However, the zeta potential of AgNPs increased as the pH value decreased because of the protonation of the carboxyl groups, which resulted in a positive surface charge of AgNPs in acidic solutions (pH 5.0 or below). The exact silver concentration in the prepared NPs dispersions was determined using ICP-MS (Fig. S2, ESI†).

### 3.2 Antibacterial activities against planktonic bacteria

Pathogenic bacteria usually present a negative surface charge whereas mammalian cells show a negligible net surface charge. In addition, an acidic microenvironment is always found in bacterial infections and in bacterial biofilms. The AgNPs have been shown to exhibit a powerful antimicrobial activity and have been widely applied in medicine because of their high antimicrobial activity and relatively good biocompatibility. Although the antibacterial mechanism of the AgNPs has not been definitively determined to date, AgNPs have a different mechanism of killing bacteria compared with the quaternary ammonium salts and other antibiotics. The results of some studies suggested that the AgNPs interact with the cell membrane and some of them also penetrate the bacterial cell wall, whereas others claimed that the antimicrobial mechanism relies on the silver ions released by the AgNPs or the formation of free radicals which induce damage to the bacterial membrane thereby causing the death of bacteria.[19] It is well accepted that the bactericidal activity of AgNPs depends on their size, shape, stability and their surface properties. In order to improve the stability and biocompatibility of AgNPs, previous researchers have used surfactants and polymers to modify the AgNPs.[20] It is speculated that AgNPs with pH induced charge switchable activities can be used to decrease cytotoxicity towards mammalian cells in neutral solutions while increasing their toxicity against bacteria in an acidic microenvironment. More importantly, the pH induced surface charge switchable AgNPs (AgNPs-LA-OB) penetrated into the bacterial biofilms and killed the bacteria embedded in the biofilms because of the negative nature of EPS and the acidic microenvironment of the biofilms.

As a proof-of-concept, the antibacterial activities of AgNPs-LA-OB against Gram-negative (*E. coli*) and Gram-positive (*S. aureus*) bacteria were evaluated using MIC and minimum bactericidal concentration (MBC) assay in a neutral or an acidic environment. The AgNPs-LA-OB were incubated with bacteria first and the proliferation of the bacteria was then monitored during 24 h of cultivation on the basis of the ODs of the suspension measured at 600 nm (OD 600) every 2 h using a UV-vis spectrometer. Additionally, the antimicrobial activities under a bacterial acidic infection site (pH 5.5) or even lower, were determined. A buffer solution with a pH value of 5.5 or 4.7 was used to simulate the

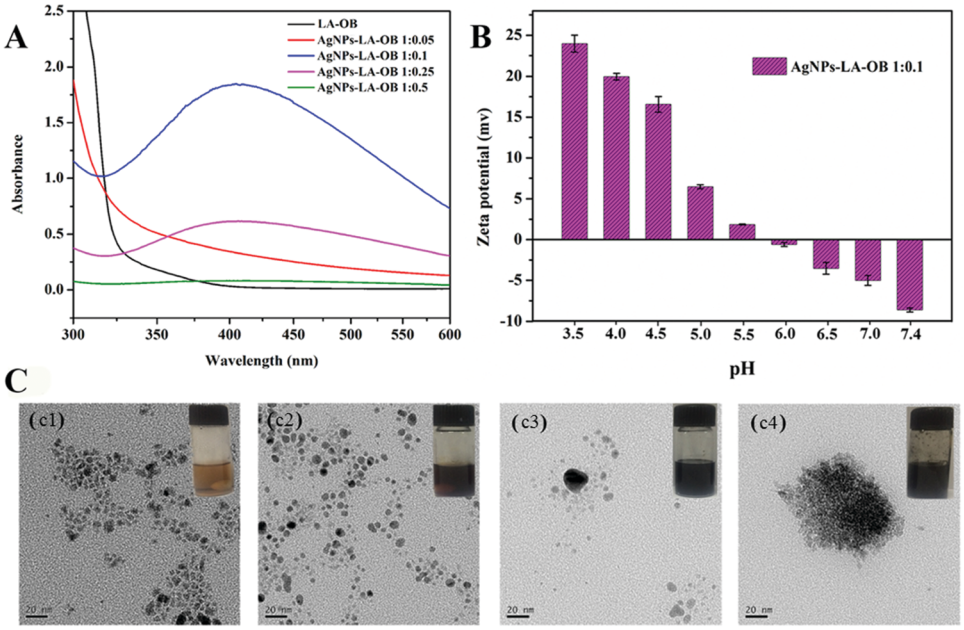


Fig. 2 (A) UV-vis absorption spectra, (B) zeta potential of AgNPs-LA-OB (1 : 0.1) at different pHs, (C) TEM micrographs of LA-OB coated AgNPs with different mass ratios, (c1) 1 : 0.05, (c2) 1 : 0.1, (c3) 1 : 0.25, (c4) 1 : 0.5 and the corresponding micrographs.

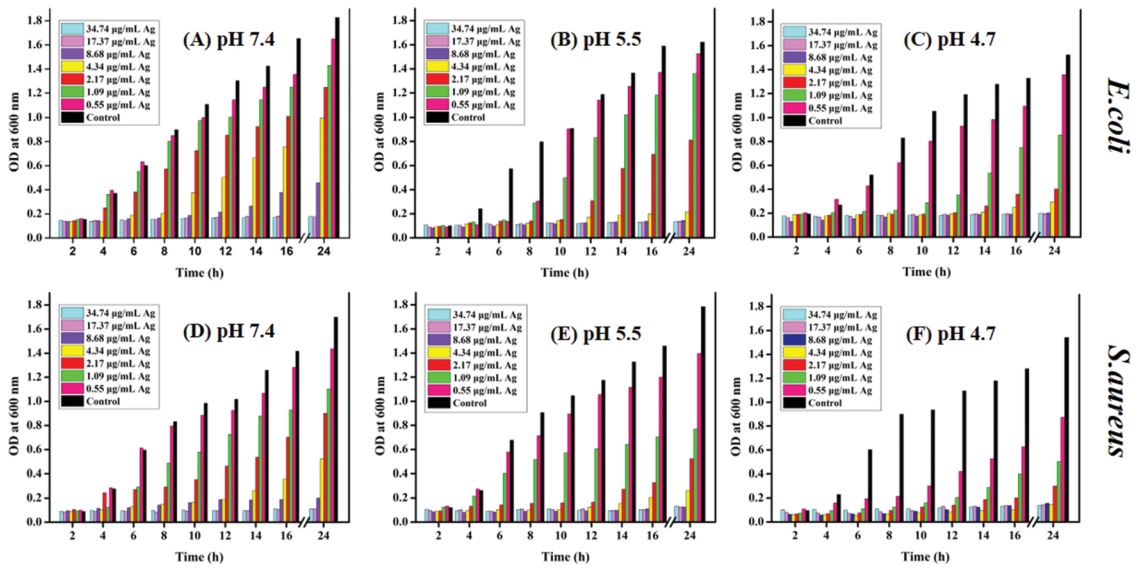


Fig. 3 Dose-dependent growth inhibition of *E. coli* (A–C) and *S. aureus* (D–F) in the presence of various concentrations of AgNPs-LA-OB as a function of time. Control: without AgNPs-LA-OB.

bacterial acidic infection tissue. The antibacterial results are presented in Fig. 3. As can be seen from Fig. 3, the MIC of AgNPs-LA-OB at pH 4.7 against *E. coli* and *S. aureus* were 1.09 μg $mL^{-1}$ and 0.55 μg $mL^{-1}$, respectively, (expressed as the total Ag concentration), which was much lower than that of AgNPs-LA-OB at pH 7.4 (4.37 μg $mL^{-1}$ and 2.17 μg $mL^{-1}$, respectively). The MIC of the nanocomposites was also determined using a microserial dilution method with tetrazolium red as indicator. Enhanced antibacterial activities were also found for AgNPs-LA-OB at an acidic solutions (pH 4.7 or pH 5.5) compared with that in neutral solutions. Antibacterial activities against planktonic bacteria of the prepared NPs at various pH values were further studied with MBC studies using a plate counting method. Fig. 4 shows the bacterial growth on agar plates with serial dilutions of AgNPs. The MBC shown is the minimum silver concentration at which no visible bacterial colonies were present on the plates. The MIC and the MBC values are summarized in Table 2. It was concluded from Fig. 4 and Table 2 that the MBCs of AgNPs-LA-OB at pH 4.7, pH 5.5 and pH 7.4 were 1.09 ppm, 2.17 ppm and 4.34 ppm, respectively,

 

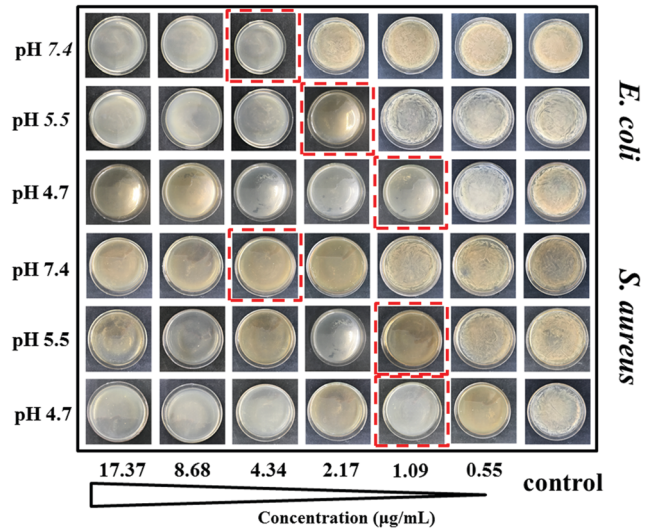


Fig. 4 Photographs of the bactericidal test in the presence of various concentrations of AgNPs-LA-OB against *S. aureus* and *E. coli* at pH 7.4, pH 5.5 or pH 4.7.

Table 2 MIC and MBC values of AgNPs-LA-OB under different pH conditions

| | MIC (ppm) | | MBC (ppm) | |
|---|---|---|---|---|
| pH value | *E. coli* | *S. aureus* | *E. coli* | *S. aureus* |
| pH 7.4 | 4.34 | 2.17 | 4.34 | 4.34 |
| pH 5.5 | 2.17 | 1.09 | 2.17 | 1.09 |
| pH 4.7 | 1.09 | 0.55 | 1.09 | 1.09 |

for *E. coli* whereas those for *S. aureus* were 1.09 ppm, 1.09 ppm and 4.34 ppm, respectively. The MBC and MIC results all demonstrated enhanced antibacterial performance at lower pH values for the pH induced surface switchable AgNPs. This pH activated enhanced antibacterial behavior could be attributed to the positive surface charge of the AgNPs-LA-OB in an acidic solution which can induce stronger interaction between AgNPs and microbes (negatively charged).

### 3.3 Visual investigation of the interaction of AgNPs-LA-OB and microbes using TEM

In order to study the interaction between the NPs and bacteria, bacteria cells incubated in the presence of AgNPs-LA-OB were examined using a TEM. The morphologies of the microorganisms before and after treatment with AgNPs-LA-OB were studied using TEM and the results are shown in Fig. 5. The *E. coli* (A) remained intact without AgNPs. However, the membranes of the bacteria had an obviously wrinkled and twisted morphology which resulted in destruction of microbes when interacted with AgNPs-LA-OB (Fig. 5B and C). Importantly, some AgNPs were adhered onto the membranes of the bacteria or penetrated into the bacteria cells, which caused visible membrane destruction and the leakage of intracellular substances. Based on these results, it was hypothesized that under an acidic infection environment, AgNPs-LA-OB exhibited a pH responsive transition from a negative charge to a positive charge which can very strongly and readily adhere on the negatively charged cell wall by means of an electrostatic

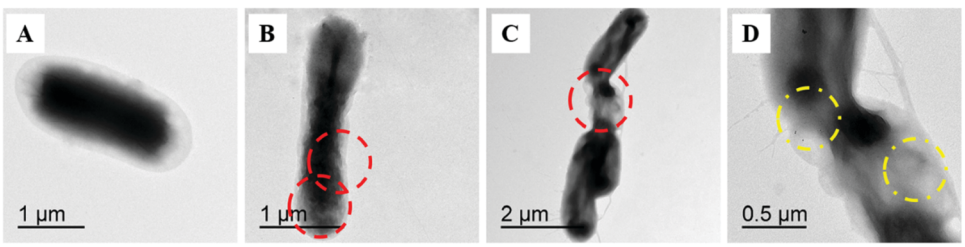


Fig. 5 Comparative TEM images of microbes of *E. coli* (A–D) in the absence (A) and presence (B–D) of AgNPs-LA-OB for 8 h. The yellow circles highlight AgNPs-LA-OB adhered to the microbial surface in (D). The rupture of the microbes' structure is highlighted by the red circles in (B and C).

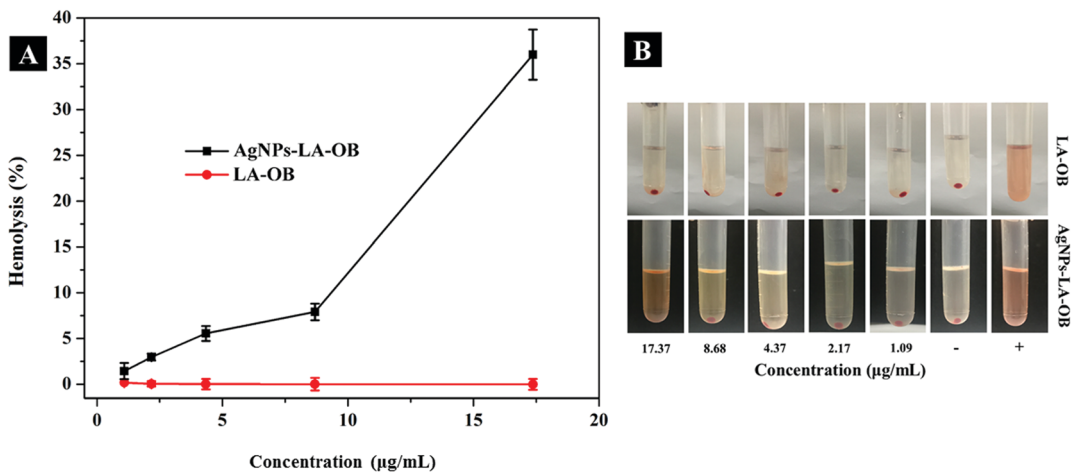


Fig. 6 Percentage of hemolysis measured using a spectrophotometer (A) and photographs of RBCs after exposure to AgNPs-LA-OB for 2 h (B).

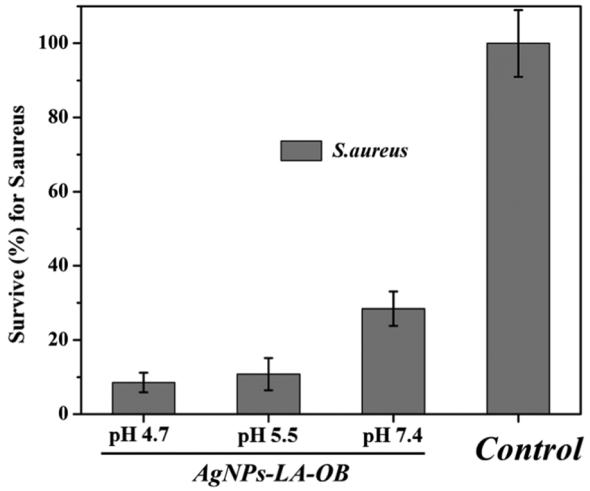


Fig. 7 Percentages of survival rates of *S. aureus* in biofilms for bacteria colonies before and after treatment with AgNPs-LA-OB.

interaction, causing the destruction of the microbial membrane and leading to cell lysis and irreversible apoptosis.

### 3.4 Hemolytic activity

The biocompatibility assay was also investigated to validate the increasing use of AgNPs in medical applications and the preliminary hemocompatibility of the prepared AgNPs-LA-OB was evaluated using a hemolysis assay. The hemoglobin released from mice RBCs after incubation with different concentrations of AgNPs-LA-OB solution was evaluated using UV-vis absorbance at a wavelength of 570 nm.

The concentration of AgNPs-LA-OB solution varies from 0.55 μg $mL^{-1}$ to 17.37 μg $mL^{-1}$ after incubation with RBCs for 2 h. The photograph of RBCs and spectrophotometric analysis of the supernatants is shown in Fig. 6. The AgNPs-LA-OB solution did not cause any observable hemoglobin release at the concentration of 4.37 μg $mL^{-1}$ which is a lethal dose to kill both Gram-negative and Gram-positive bacteria and is far lower than those reported in the literature for bacteria of the same size.[59,60] The large, negatively charged surface of the small AgNPs may account for the low hemolysis activity. Although the AgNPs-LA-OB solution efficiently disrupts the microbial walls/membranes under the infection site, it does not damage the RBC membranes in healthy tissues which was attributed to the pH responsive zwitterionic charge of the AgNPs. Therefore, AgNPs-LA-OB showed satisfactory selectivity for bacterial cells over RBCs.

### 3.5 Antibiofilm activities of AgNPs-LA-OB

AgNP–LA-OB dispersed into PBS with a pH of 7.4, 5.5 and 4.7 resulted in AgNP–LA-OB with different surface charges. A seven day old *S. aureus* biofilm was treated with 200 μL of AgNP–LA-OB solutions for 16 h. A standard plate counting assay, Live/Dead staining assay and SEM observation were used to evaluate the antibiofilm activities of AgNP–LA-OB in different acidic microenvironments. The standard plate counting assay (Fig. 7) illustrated that about 30% bacteria survive after 16 h treatment with AgNP–LA-OB at pH 7.4 whereas less than 10% bacteria survive at treatment in acidic solutions, indicating the outstanding bactericidal activities of AgNP–LA-OB under acidic environment as a result of a surface charge switch to positive in acidic solutions. The antibiofilm activities of AgNP–LA-OB were further examined visually using CLSM observation of cells stained with a LIVE/DEAD Biofilm Viability kit. The live bacteria with intact cell membranes displayed a green fluorescence and the dead bacteria with damaged cell membranes showed red fluorescence in the CLSM images. As shown in Fig. 8, untreated controls were characterized by intact

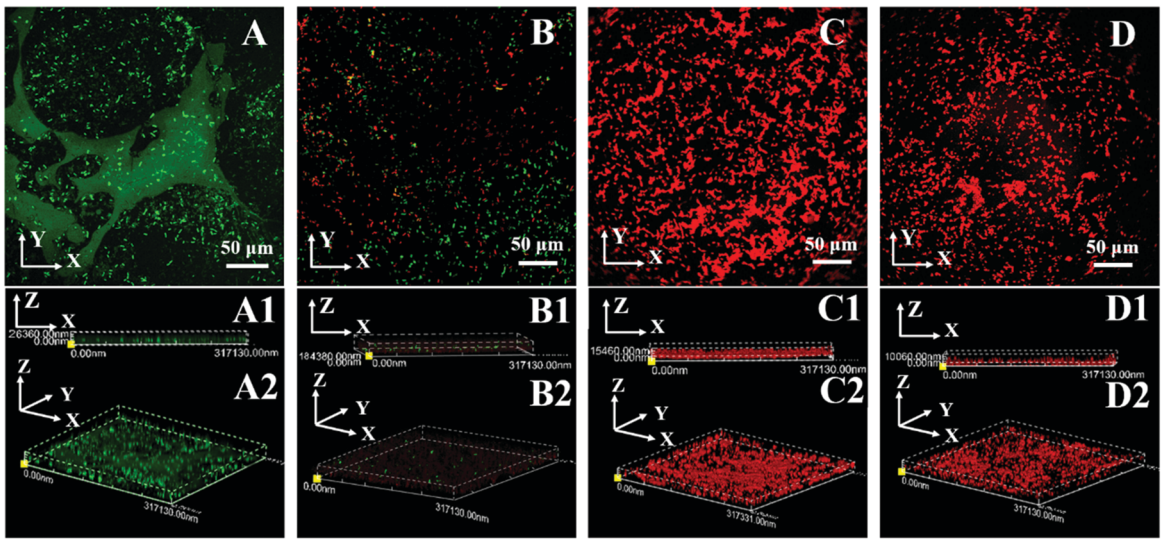


Fig. 8 The confocal microscopy images of *S. aureus* biofilms before treatment with AgNPs-LA-OB (A) and treatment with AgNPs-LA-OB at pH 7.4 (B), pH 5.5 (C) and pH 4.7 (D) after 16 h incubation were stained using LIVE/DEAD BacLight Bacterial Viability kits. Live (green) and dead (red) bacteria were imaged using CLSM. Images A, B, C and D show the top view and images A1, A2, B1, B2, C1, C2, D1, D2 are three-dimensional reconstructions of z-stacks collected across the biofilm thickness. Scale bars: 50 μm.

 

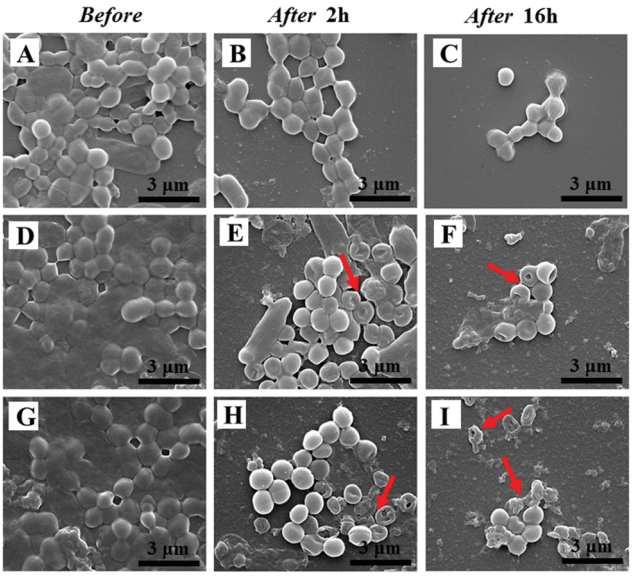


Fig. 9 SEM images of *S. aureus* biofilms treated with PBS at a pH of 7.4 (A), 5.5 (D) and 4.7 (G); after treatment with AgNPs-LA-OB at pH 7.4 for 2 h (B) and 16 h (C); after treatment with AgNPs-LA-OB at pH 5.5 for 2 h (E) and 16 h (F); after treatment with AgNPs-LA-OB at pH 4.7 for 2 h (H) and 16 h (I).

biofilms with entirely live (green) bacteria across the whole biofilm. Biofilms treated with AgNP–LA-OB at pH 7.4 (Fig. 8B) illustrated partial cell death (red). Notably, AgNP–LA-OB at acidic solutions (pH 4.7 and pH 5.5) killed bacteria throughout the full biofilm thickness (Fig. 8C and D), suggesting that there had been penetration throughout the biofilms and excellent killing efficiency of AgNP–LA-OB at an acidic environment as a result of acidic induced surface charge transform activities. SEM was used to directly examine visually the antibiofilm efficiency of AgNP–LA-OB in neutral (pH 7.4) and acidic (pH 5.5 and pH 4.7) solutions for 2 h and 16 h and the results are given in Fig. 9. After treatment with AgNP–LA-OB at acidic solutions (pH 4.7 and pH 5.5), the *S. aureus* biofilm presented obvious structural destruction (Fig. 9E, F, H and I), and all of the bacteria were killed. As controls, the *S. aureus* biofilm treated with AgNP–LA-OB in neutral conditions showed less bactericidal effects than that in acidic solutions.

## 4. Conclusions

In summary, the AgNPs surface coated with carboxyl betaine (CB) groups (AgNPs-LA-OB) were prepared and resulted in the NPs with pH induced surface charge switchable activities. The zwitterion nature and negative surface charge of AgNPs-LA-OB at normal physiological conditions resulted in an improved cytocompatibility toward mammalian cells. The positive charge of AgNPs-LA-OB in an acidic fluid, which is characteristic for bacterial infections, rendered the NPs with improved killing activities towards both bacteria planktonic and bacteria embedded in biofilms, not only through the enhanced adhesion of AgNPs to the bacterial membrane, but also because of the deep penetration of the particles within the bacterial biofilm. Therefore, the AgNPs-LA-OB can be potentially used as new antibacterial materials to combat bacterial infections of their biofilms.

## Conflicts of interest

There are no conflicts to declare.

## Acknowledgements

This work was financially supported by the Applied Basic Research Programs Foundation of Sichuan Province (No. 2015JY0126) and by the Functional Polymer Innovation Team Project, Southwest Minzu University (No. 14CXTD04).

## References

1 J. Song, H. Kim and Y. Jang, *et al.*, Enhanced antibacterial activity of silver/polyrhodanine-composite-decorated silica nanoparticles, *ACS Appl. Mater. Interfaces*, 2013, **5**(22), 11563–11568.
2 Y. Qiao, F. Ma and C. Liu, *et al.*, Near-Infrared Laser-Excited Nanoparticles To Eradicate Multidrug-Resistant Bacteria and Promote Wound Healing, *ACS Appl. Mater. Interfaces*, 2017, **10**(1), 193–206.
3 L. Timofeeva and N. Kleshcheva, Antimicrobial polymers: mechanism of action, factors of activity, and applications, *Appl. Microbiol. Biotechnol.*, 2011, **89**(3), 475–492.
4 K. E. Jones, N. G. Patel and M. A. Levy, *et al.*, Global trends in emerging infectious diseases, *Nature*, 2008, **451**(7181), 990–993.
5 J. Davies and D. Davies, Origins and evolution of antibiotic resistance, *Microbiol. Mol. Biol. Rev.*, 2010, **74**(3), 417–433.
6 C. A. Arias and B. E. Murray, A new antibiotic and the evolution of resistance, *N. Engl. J. Med.*, 2015, **372**(12), 1168–1170.
7 T. R. Frieden, The future of public health, *N. Engl. J. Med.*, 2015, **373**(18), 1748–1754.
8 Y. Kuthati, R. K. Kankala and S. X. Lin, *et al.*, pH-triggered controllable release of silver–indole-3 acetic acid complexes from mesoporous silica nanoparticles (IBN-4) for effectively killing malignant bacteria, *Mol. Pharmaceutics*, 2015, **12**(7), 2289–2304.
9 A. Giedraitienė, A. Vitkauskienė and R. Naginienė, *et al.*, Antibiotic resistance mechanisms of clinically important bacteria, *Medicina*, 2011, **47**(3), 137–146.
10 I. A. Dan and D. Hughes, Persistence of antibiotic resistance in bacterial populations, *FEMS Microbiol. Rev.*, 2011, **35**(5), 901–911.
11 D. Liu, L. Ma and L. Liu, *et al.*, Polydopamine-encapsulated Fe3O4 with an adsorbed HSP70 inhibitor for improved photothermal inactivation of bacteria, *ACS Appl. Mater. Interfaces*, 2016, **8**(37), 24455–24462.
12 D. I. Andersson and D. Hughes, Antibiotic resistance and its cost: is it possible to reverse resistance?, *Nat. Rev. Microbiol.*, 2010, **8**(4), 260–271.

13 F. Huang, Y. Gao and Y. Zhang, *et al.*, Silver-decorated polymeric micelles combined with curcumin for enhanced antibacterial activity, *ACS Appl. Mater. Interfaces*, 2017, **9**(20), 16880–16889.
14 X. Ding, S. Duan and X. Ding, *et al.*, Versatile antibacterial materials: An emerging arsenal for combatting bacterial pathogens, *Adv. Funct. Mater.*, 2018, **28**(40), 1802140.
15 T. Wei, Q. Yu and W. Zhan, *et al.*, A Smart Antibacterial Surface for the On-Demand Killing and Releasing of Bacteria, *Adv. Healthcare Mater.*, 2016, **5**(4), 449–456.
16 Q. Yu, Z. Wu and H. Chen, Dual-function antibacterial surfaces for biomedical applications, *Acta Biomater.*, 2015, **16**(1), 1–13.
17 K. Zou, Q. Liu and J. Chen, *et al.*, Silver-decorated biodegradable polymer vesicles with excellent antibacterial efficacy, *Polym. Chem.*, 2013, **5**(2), 405–411.
18 W. Bing, Z. Chen and H. Sun, *et al.*, Visible-light-driven enhanced antibacterial and biofilm elimination activity of graphitic carbon nitride by embedded Ag nanoparticles, *Nano Res.*, 2015, **8**(5), 1648–1658.
19 J. Liu and R. H. Hurt, Ion release kinetics and particle persistence in aqueous nano-silver colloids, *Environ. Sci. Technol.*, 2010, **44**(6), 2169–2175.
20 S. Kittler, C. Greulich and J. Diendorf, *et al.*, Toxicity of silver nanoparticles increases during storage because of slow dissolution under release of silver ions, *Chem. Mater.*, 2010, **22**(16), 4548–4554.
21 B. Le Ouay and F. Stellacci, Antibacterial activity of silver nanoparticles: a surface science insight, *Nano Today*, 2015, **10**(3), 339–354.
22 J. R. Morones, J. L. Elechiguerra and A. Camacho, *et al.*, The bactericidal effect of silver nanoparticles, *Nanotechnology*, 2005, **16**(10), 2346–2353.
23 S. Silver, Bacterial silver resistance: molecular biology and uses and misuses of silver compounds, *FEMS Microbiol. Rev.*, 2003, **27**(2–3), 341–353.
24 M. Mahmoudi and V. Serpooshan, Silver-coated engineered magnetic nanoparticles are promising for the success in the fight against antibacterial resistance threat, *ACS Nano*, 2012, **6**(3), 2656–2664.
25 Y. Su, L. Zhao and F. Meng, *et al.*, Silver nanoparticles decorated lipase-sensitive polyurethane micelles for on-demand release of silver nanoparticles, *Colloids Surf., B*, 2017, **152**, 238–244.
26 Y. Yao, D. Xu and C. Liu, *et al.*, Biodegradable pH-sensitive polyurethane micelles with different polyethylene glycol (PEG) locations for anti-cancer drug carrier applications, *RSC Adv.*, 2016, **6**(100), 97684–97693.
27 B. M. Geilich, I. Gelfat, S. Sridhar, A. L. van de Ven and T. J. Webster, Superparamagnetic iron oxide-encapsulating polymersome nanocarriers for biofilm eradication, *Biomaterials*, 2017, **119**, 78–85.
28 P. Liu, G. Xu and D. Pranantyo, *et al.*, pH-Sensitive Zwitterionic Polymer as an Antimicrobial Agent with Effective Bacterial Targeting, *ACS Biomater. Sci. Eng.*, 2017, **4**(1), 40–46.
29 S. Yan, H. Shi and L. Song, *et al.*, Nonleaching Bacteria-Responsive Antibacterial Surface Based on a Unique Hierarchical Architecture, *ACS Appl. Mater. Interfaces*, 2016, **8**(37), 24471–24481.
30 S. Yuan, Y. Li and S. Luan, *et al.*, Infection-resistant styrenic thermoplastic elastomers that can switch from bactericidal capability to anti-adhesion, *J. Mater. Chem. B*, 2016, **4**(6), 1081–1089.
31 B. Horev, M. I. Klein and G. Hwang, *et al.*, pH-activated nanoparticles for controlled topical delivery of farnesol to disrupt oral biofilm virulence, *ACS Nano*, 2015, **9**(3), 2390–2404.
32 T. O. Peulen and K. J. Wilkinson, Diffusion of nanoparticles in a biofilm, *Environ. Sci. Technol.*, 2011, **45**(8), 3367–3373.
33 J. W. Costerton, P. S. Stewart and E. P. Greenberg, Bacterial biofilms: a common cause of persistent infections, *Science*, 1999, **284**(5418), 1318–1322.
34 X. Li, Y. C. Yeh and K. Giri, *et al.*, Control of nanoparticle penetration into biofilms through surface design, *Chem. Commun.*, 2015, **51**(2), 282–285.
35 D. Hu, H. Li and B. Wang, *et al.*, Surface-adaptive gold nanoparticles with effective adherence and enhanced photothermal ablation of methicillin-resistant staphylococcus aureus biofilm, *ACS Nano*, 2017, **11**(9), 9330–9339.
36 Y. Su, L. Zhao and F. Meng, *et al.*, Triclosan loaded polyurethane micelles with pH and lipase sensitive properties for antibacterial applications and treatment of biofilms, *Mater. Sci. Eng., C*, 2018, **93**, 921–930.
37 Y. Guan, Y. Su and L. Zhao, *et al.*, Biodegradable polyurethane micelles with pH and reduction responsive properties for intracellular drug delivery, *Mater. Sci. Eng., C*, 2017, **75**, 1221–1230.
38 Y. Zhong, C. Wang and L. Cheng, *et al.*, Gold nanorod-cored biodegradable micelles as a robust and remotely controllable doxorubicin release system for potent inhibition of drug-sensitive and-resistant cancer cells, *Biomacromolecules*, 2013, **14**(7), 2411–2419.
39 Y. Lu, J. Jiang and S. Yoon, *et al.*, High-Performance Stretchable Conductive Composite Fibers from Surface-Modified Silver Nanowires and Thermoplastic Polyurethane by Wet Spinning, *ACS Appl. Mater. Interfaces*, 2018, **10**(2), 2093–2104.
40 D. Kaewwichit, V. Aksornkitti and R. Rojanathanes, *et al.*, Synthesis and structure-property relationship of lipoic acid-containing porphyrin derivatives for mitochondria-targeting applications, *Inorg. Chim. Acta*, 2018, **471**, 305–309.
41 A. Sadownik, J. Stefely and S. L. Regen, Polymerized liposomes formed under extremely mild conditions, *J. Am. Chem. Soc.*, 1986, **108**(24), 7789–7791.
42 Y. Jiang, Y. Su and L. Zhao, *et al.*, Preparation and antifouling properties of 2-(meth-acryloyloxy)ethyl cholinephosphate based polymers modified surface with different molecular architectures by ATRP, *Colloids Surf., B*, 2017, **156**, 87–94.
43 I. Wiegand, K. Hilpert and R. E. W. Hancock, Agar and broth dilution methods to determine the minimal inhibitory concentration (MIC) of antimicrobial substances, *Nat. Protoc.*, 2008, **3**(2), 163–175.
44 F. Meng, Z. Qiao and Y. Yao, *et al.*, Synthesis of polyurethanes with pendant azide groups attached on the soft segments

 

and the surface modification with mPEG by click chemistry for antifouling applications, *RSC Adv.*, 2018, **8**(35), 19642–19650.

45 L. H. Kim, Y. Jung and H. W. Yu, *et al.*, Physicochemical interactions between rhamnolipids and Pseudomonas aeruginosa biofilm layers, *Environ. Sci. Technol.*, 2015, **49**(6), 3718–3726.

46 S. Goswami, D. Thiyagarajan and G. Das, *et al.*, Biocompatible nanocarrier fortified with a dipyridinium-based amphiphile for eradication of biofilm, *ACS Appl. Mater. Interfaces*, 2014, **6**(18), 16384–16394.

47 X. Wang, A. Deng and W. Cao, *et al.*, Synthesis of chitosan/poly (ethylene glycol)-modified magnetic nanoparticles for antibiotic delivery and their enhanced anti-biofilm activity in the presence of magnetic field, *J. Mater. Sci.*, 2018, **53**(9), 6433–6449.

48 W. Zhou, Z. Jia and P. Xiong, *et al.*, Bioinspired and biomimetic AgNPs/gentamicin-embedded silk fibroin coatings for robust antibacterial and osteogenetic applications, *ACS Appl. Mater. Interfaces*, 2017, **9**(31), 25830–25846.

49 J. Li, K. Zhang and L. Ruan, *et al.*, Block copolymer nanoparticles remove biofilms of drug-resistant Gram-positive bacteria by nanoscale bacterial debridement, *Nano Lett.*, 2018, **18**(7), 4180–4187.

50 R. M. Gouveia, E. González-Andrades and J. C. Cardona, *et al.*, Controlling the 3D architecture of Self-Lifting Auto-generated Tissue Equivalents (SLATEs) for optimized corneal graft composition and stability, *Biomaterials*, 2017, **121**, 205–219.

51 H. Cui, H. Zhou and L. Lin, The specific antibacterial effect of the Salvia oil nanoliposomes against Staphylococcus aureus, biofilms on milk container, *Food Control*, 2016, **61**, 92–98.

52 Q. Guo, Y. Zhao and X. Dai, *et al.*, Functional silver nanocomposites as broad-spectrum antimicrobial and biofilm-disrupting agents, *ACS Appl. Mater. Interfaces*, 2017, **9**(20), 16834–16847.

53 D. Xu, Y. Su and L. Zhao, *et al.*, Antibacterial and antifouling properties of a polyurethane surface modified with perfluoroalkyl and silver nanoparticles, *J. Biomed. Mater. Res., Part A*, 2017, **105**(2), 531–538.

54 F. Nederberg, Y. Zhang and J. P. K. Tan, *et al.*, Biodegradable nanostructures with selective lysis of microbial membranes, *Nat. Chem.*, 2011, **3**(5), 409–414.

55 Y. Xi, T. Song and S. Tang, *et al.*, Preparation and antibacterial mechanism insight of polypeptide-based micelles with excellent antibacterial activities, *Biomacromolecules*, 2016, **17**(12), 3922–3930.

56 J. Choi, V. Reipa and V. M. Hitchins, *et al.*, Physicochemical Characterization and In Vitro Hemolysis Evaluation of Silver Nanoparticles, *Toxicol. Sci*, 2011, **123**(1), 133–143.

57 M. A. Dobrovolskaia, J. D. Clogston and B. W. Neun, *et al.*, Method for analysis of nanoparticle hemolytic properties in vitro, *Nano Lett.*, 2008, **8**(8), 2180–2187.

58 Y. S. Lin and C. L. Haynes, Impacts of mesoporous silica nanoparticle size, pore ordering, and pore integrity on hemolytic activity, *J. Am. Chem. Soc.*, 2010, **132**(13), 4834–4842.

59 L. Q. Chen, L. Fang and J. Ling, *et al.*, Nanotoxicity of silver nanoparticles to red blood cells: size dependent adsorption, uptake, and hemolytic activity, *Chem. Res. Toxicol.*, 2015, **28**(3), 501–509.

60 L. Liu, J. Yang and J. Xie, *et al.*, The potent antimicrobial properties of cell penetrating peptide-conjugated silver nanoparticles with excellent selectivity for Gram-positive bacteria over erythrocytes, *Nanoscale*, 2013, **5**(9), 3834–3840.